ORIGINAL ARTICLE

Journal of Cachexia, Sarcopenia and Muscle 2023; **14**: 2882–2897
Published online 15 November 2023 in Wiley Online Library (wileyonlinelibrary.com) **DOI:** 10.1002/jcsm.13349

Ryanodine receptor type 1 content decrease-induced endoplasmic reticulum stress is a hallmark of myopathies

Jeremy Vidal[1], Eric A. Fernandez[2], Martin Wohlwend[3], Pirkka-Pekka Laurila[4], Andrea Lopez-Mejia[2], Julien Ochala[5], Alexander J. Lobrinus[6,7], Bengt Kayser[1], Isabel C. Lopez-Mejia[2], Nicolas Place[1] & Nadège Zanou[1]*

[1]*Institute of Sport Sciences and Department of Biomedical Sciences, University of Lausanne, Lausanne, Switzerland;* [2]*Center for Integrative Genomics, University of Lausanne, Lausanne, Switzerland;* [3]*Computer Science and Artificial Intelligence Laboratory, Massachusetts Institute of Technology, Cambridge, Massachusetts, USA;* [4]*Helsinki University Central Hospital, Helsinki, Finland;* [5]*Department of Biomedical Sciences, University of Copenhagen, Copenhagen, Denmark;* [6]*Institute of Pathology, Lausanne University Hospital (CHUV), Lausanne, Switzerland;* [7]*Department of Clinical Pathology, University Hospital Geneva, Geneva, Switzerland*

Abstract

Background Decreased ryanodine receptor type 1 (RyR1) protein levels are a well-described feature of recessive *RYR1*-related myopathies. The aim of the present study was twofold: (1) to determine whether RyR1 content is also decreased in other myopathies and (2) to investigate the mechanisms by which decreased RyR1 protein triggers muscular disorders.

Methods We used publicly available datasets, muscles from human inflammatory and mitochondrial myopathies, an inducible muscle-specific *RYR1* recessive mouse model and RyR1 knockdown in C2C12 muscle cells to measure RyR1 content and endoplasmic reticulum (ER) stress markers. Proteomics, lipidomics, molecular biology and transmission electron microscopy approaches were used to decipher the alterations associated with the reduction of RyR1 protein levels.

Results *RYR1* transcripts were reduced in muscle samples of patients suffering from necrotizing myopathy ($P = 0.026$), inclusion body myopathy ($P = 0.003$), polymyositis ($P < 0.001$) and juvenile dermatomyositis ($P < 0.001$) and in muscle samples of myotonic dystrophy type 2 ($P < 0.001$), presymptomatic ($P < 0.001$) and symptomatic ($P < 0.001$) Duchenne muscular dystrophy, Becker muscular dystrophy ($P = 0.004$) and limb-girdle muscular dystrophy type 2A ($P = 0.004$). RyR1 protein content was also significantly decreased in inflammatory myopathy (−75%, $P < 0.001$) and mitochondrial myopathy (−71%, $P < 0.001$) muscles. Proteomics data showed that depletion of RyR1 protein in C2C12 myoblasts leads to myotubes recapitulating the common molecular alterations observed in myopathies. Mechanistically, RyR1 protein depletion reduces ER–mitochondria contact length (−26%, $P < 0.001$), Ca^{2+} transfer to mitochondria (−48%, $P = 0.002$) and the mitophagy gene Parkinson protein 2 transcripts ($P = 0.037$) and induces mitochondrial accumulation (+99%, $P = 0.005$) and dysfunction ($P < 0.001$). This was associated to the accumulation of deleterious sphingolipid species. Our data showed increased levels of the ER stress marker chaperone-binding protein/glucose regulated protein 78, GRP78-Bip, in RyR1 knockdown myotubes (+45%, $P = 0.046$), in mouse RyR1 recessive muscles (+58%, $P = 0.001$) and in human inflammatory (+96%, $P = 0.006$) and mitochondrial (+64%, $P = 0.049$) myopathy muscles. This was accompanied by increased protein levels of the pro-apoptotic protein CCAAT-enhancer-binding protein homologous protein, CHOP-DDIT3, in RyR1 knockdown myotubes (+27%, $P < 0.001$), mouse RyR1 recessive muscles (+63%, $P = 0.009$), human inflammatory (+50%, $P = 0.038$) and mitochondrial (+51%, $P = 0.035$) myopathy muscles. In publicly available datasets, the decrease in *RYR1* content in myopathies was also associated to increased ER stress markers and *RYR1* transcript levels are inversely correlated with ER stress markers in the control population.

Conclusions Decreased RyR1 is commonly observed in myopathies and associated to ER stress in vitro, in mouse muscle and in human myopathy muscles, suggesting a potent role of RyR1 depletion-induced ER stress in the pathogenesis of myopathies.

Keywords calcium; CHOP; GRP78-Bip; lipid droplet; mitophagy; muscle

Received: 8 March 2023; Revised: 24 July 2023; Accepted: 11 September 2023
**Correspondence to: Nadège Zanou, Institute of Sport Sciences and Department of Biomedical Sciences, University of Lausanne, Lausanne, Switzerland. Email: nadege.zanou@unil.ch*

Introduction

Ryanodine receptor type 1 (RyR1), the largest known homotetramer, with a total molecular mass > 2 MDa, is involved in muscle contraction.[1] While exercise-induced acute RyR1 Ca^{2+} leak promotes positive mitochondrial adaptations,[2] sustained Ca^{2+} leak from the RyR1 channel has been linked to several pathological conditions, such as myopathies, cachexia or sarcopenia.[3–5] RyR1 function can also be altered by mutations, which trigger the so-called RyR1-related myopathies (*RYR1*-RMs). *RYR1*-RMs constitute the most common class of congenital myopathies, including central core disease, multicore disease, core-rod myopathy, centronuclear myopathy and congenital fibre-type disproportion.[6] RyR1 mutations can be either homozygous or heterozygous and lead to distinct defects ranging from leaky RyR1, excitation–contraction uncoupling, to the loss of RyR1 protein, the latter being caused by recessive RyR1 mutations. Attempts to study how *RYR1* recessive mutations reducing RyR1 protein levels induce myopathies have proved difficult. Indeed, complete deletion of *RYR1* in vivo is lethal, making it difficult to study the role of RyR1 protein depletion in the pathogenesis of myopathies.

An inducible muscle-specific *RYR1* knock-out mouse model (RyR1-Rec) has been recently developed[7] and demonstrated that a 50% RyR1 protein reduction is sufficient to induce muscle disease. Whether RyR1 protein decrease might also be associated to other myopathies is unknown, and whether the decrease in RyR1 protein specifically triggers these disorders remains poorly understood. A previous study has reported in inclusion body myositis (IBM), a severe form of inflammatory myopathy (IM) with no mutations on *RYR1*, a decrease in the levels of RyR1 protein, among other Ca^{2+} channel proteins, and this was associated to increased endoplasmic reticulum (ER) stress markers,[8] but the specific role of RyR1 protein decrease in the induction of ER stress in IBM has not been investigated.

ER stress is triggered by the accumulation of misfolded proteins and damaged lipids or by Ca^{2+} imbalance. Activation of ER stress has been shown as a central mechanism of the pathogenesis of obesity and peripheral insulin resistance,[9] and increasing evidence shows association of ER stress with myopathies.[8,10,11] ER stress triggers a physiological response called the unfolded protein response (UPR). UPR activation is regulated by three distinct transmembrane proteins and their signalling pathways: the pancreatic ER kinase (PRK)-like ER kinase (PERK), the activating transcription factor 6 (ATF6) and the inositol-requiring enzyme 1 alpha (IRE1α).[11] In normal conditions, these transmembrane proteins are inactivated by the chaperone-binding protein/glucose regulated protein 78 (GRP78-Bip).[12] In response to ER stress, GRP78-Bip dissociates from the transmembrane proteins and binds misfolded proteins, leading to the activation of the UPR response. Accordingly, an increase in GRP78-Bip levels has been reported as a strong marker of ER stress.[13] ER stress leads to the activation of pro-survival factors, such as phosphorylation of the eukaryotic initiation factor 2 alpha (eIF2α) to promote a pro-adaptive signalling pathway by the inhibition of global protein synthesis and selective translation of activating transcription factor 4 (ATF4).[14] During conditions of prolonged ER stress, pro-adaptive responses fail and apoptotic cell death ensues by the pro-apoptotic protein CCAAT-enhancer-binding protein homologous protein, CHOP-DDIT3. This leads to the induction of several pro-apoptotic genes and suppression of the synthesis of anti-apoptotic Bcl-2 proteins.[14]

Several reasons render the endo/sarcoplasmic reticulum (ER/SR) a key organelle for counteracting cellular stress. First, its abundant membrane compartments form contact sites with other cellular compartments—such as the nuclear envelope, the endosomes, Golgi apparatus, mitochondria, lipid droplets (LDs), plasma membrane, lysosomes and peroxisomes—which are key to reduce ER stress.[15] For example, ER contact sites with mitochondria form an exchange space called mitochondria-associated membranes (MAMs). MAMs allow a direct transfer of Ca^{2+} from the ER to the mitochondria by connecting the voltage-dependent anionic channel (VDAC) on the mitochondrial outer membrane to the inositol-1,4,5-triphosphate receptor (IP3R) on the ER membrane.[16] Alterations to this process disturb ER Ca^{2+} homeostasis.[11] The ER is also responsible for the formation of mitophagosomes, where damaged mitochondria are ubiquitinated and dynamically encased[17] to be degraded by a process called mitophagy. Mitophagy is a quality control mechanism that ensures the elimination of damaged mitochondria[18] and plays a key role in muscle homeostasis.

During mitophagy, the proautophagic protein BECN1/Beclin1 interacts with PTEN-induced putative kinase 1, PINK1, which relocalizes to the MAMs.[19] Impaired mitophagy triggers the accumulation of defective and non-functional mitochondria, which appear elongated.[20] A potential role of RyR1 in regulating the mitophagy process has not been previously reported.

In the present study, combining bioinformatics, proteomics, lipidomics, molecular biology and imaging, we aimed to investigate whether RyR1 protein decrease might also be associated to non-*RYR1*-RMs and to decipher the molecular mechanisms by which RyR1 protein depletion induces muscular disorders.

Materials and methods

Detailed materials and methods are described in the supporting information.

Ethical approval

Our research complies with all relevant ethical regulations; the study was validated by the Commission d'éthique de la recherche sur l'être humain du Canton de Vaud with the reference CER-VD 2019-00356.

Human muscle biopsies

All the human muscle biopsies were obtained from the Institut Universitaire de Pathologie and the Biobanque of the Canton de Vaud, where a clear diagnosis was established for each patient. All the subjects provided consent in exploiting their sample for research purposes. IM (n = 5, 4 quadriceps and 1 deltoid samples) and mitochondrial myopathy (MM) (n = 5, 4 deltoid and 1 quadriceps samples) were compared with age-matched healthy control muscles (n = 4, 2 quadriceps and 2 deltoid samples).

Muscle biopsies examination

The main diagnostic criterion for IMs was the presence of endomysial or perimysial lymphocytic infiltrates, with or without muscle fibres necrosis. For IBM, the presence of rimmed vacuoles and TDP43-positive inclusions was required.

The diagnostic criterion for MM was the presence of ragged red fibres with COX-negative muscle fibres.

Human muscle gene expression analysis

Gene expression data for different muscular dystrophies (control, n = 18; Becker muscular dystrophy, n = 5; Duchenne muscular dystrophy [DMD], n = 10; juvenile dermatomyositis [JDM], n = 21; limb-girdle muscular dystrophy 2A [LGMD2A], n = 10) were obtained from the publicly available dataset E-GEOD-3307.[21] Gene expression data for different inflammatory myositis disorders (control, n = 5; dermatomyositis, n = 8; polymyositis, n = 8; necrotizing myositis, n = 5; IBM, n = 10) were retrieved from the publicly available dataset GSE39454.[22] *RYR1* expression levels in skeletal muscle of control (n = 10) or myotonic dystrophy 2 (DM2) patients (n = 10) were obtained from GSE37084[23] whereas *RYR1* muscle expression levels of control (n = 14) and presymptomatic DMD children (n = 23) were obtained from GSE6011.[24] Preprocessed data were used for data analysis. Heatmaps are shown as log2 fold change of each muscle disease relative to controls and *P*-values obtained from online Expression Atlas of the datasets. Gene expression correlations from post-mortem skeletal muscle biopsies were performed using the Genotype-Tissue Expression (GTEx) project v7, n = 491, and Pearson's correlations.

Mouse model

An inducible RyR1 recessive (RyR1-Rec) mouse was generated as previously reported.[25,26] Briefly, $RyR1^{flox/flox}$ mice (C57BL/6J background) with LoxP sites flanking exons 9–11 of the *RYR1* gene were crossed with the HSA-Cre-ER^{T2} mice.[26] This generates the $RyR1^{flox/flox}$::HSA-Cre-ER^{T2} mouse line. Tamoxifen injection was performed five consecutive days intraperitoneally in 2-month male mice to inactivate RyR1. Mice were given ad libitum access to food and water, and food pellets were provided directly in the cage to ensure a correct feeding. Mice were kept for 75 days before sacrifice.

Cell culture

C2C12 mouse skeletal myoblasts were obtained from the American Type Culture Collection and grown in proliferation medium composed of Dulbecco's modified Eagle's medium (DMEM; Cat 11995065) supplemented with 10% foetal bovine serum, 100 IU/mL of penicillin, 100 μg/mL of streptomycin and 1% non-essential amino acids (all from Thermo Fisher Scientific, Basel, Switzerland) and maintained at 37°C in a humidified atmosphere with 5% CO_2. To induce differentiation, myoblasts were grown to 80–90% confluence, and the proliferation medium was then replaced by a differentiation medium (DM), consisting of DMEM supplemented with 2% horse serum (Thermo Fisher Scientific).

Small interfering RNA transfection

To perform the small interfering RNA (siRNA) transfection, ~150 000 C2C12 myoblasts were plated per well of a

six-well plate. Twenty-four hours after seeding, the myoblasts were transfected with 10, 50 or 100 nM of silencer select negative control siRNA (si-CTRL) (4390843, Thermo Fisher Scientific) or silencer select pre-designed siRNA directed against RyR1 (si-RyR1) (B1, s73237 or B2, s73238, Thermo Fisher Scientific) using Lipofectamine RNAiMAX according to the manufacturer (Thermo Fisher Scientific). The differentiation was induced the day after the transfection and the analyses were performed at Day 4 post-transfection and Day 3 of differentiation (D4TD3D) or at Day 7 post-transfection and Day 6 of differentiation (D7TD6D).

Statistical analyses

Except for proteomic and lipidomic analyses, data are presented as mean ± SD. Statistical significance was determined using Student's two-tailed *t*-tests or Kolmogorov–Smirnov's tests (when normality fails) to compare two groups. To compare more than two groups, we used one-way analysis of variance (ANOVA) followed by Dunnett's multiple-comparisons post hoc tests.

For the correlogram, Pearson's correlations and Student's *P*-values were calculated using the corAndPvalue function in WGCNA package, R Bioconductor. Other data were analysed using GraphPad Prism Version 8.4.2. The level of significance was fixed at $P \leq 0.05$.

Results

Ryanodine receptor type 1 transcript levels are decreased in various human myopathies

We used publicly available datasets to analyse the abundance of *RYR1* transcripts in skeletal muscle of patients suffering from various myopathies and compared them with healthy controls. We found a significant decrease in *RYR1* transcripts in (1) IM, necrotizing myopathy ($P = 0.026$), IBM ($P = 0.003$), polymyositis ($P < 0.001$) (*Figure 1A*) and JDM ($P < 0.001$) (*Figure 1B*) and (2) muscular dystrophies, DM2 ($P < 0.001$) (*Figure 1C*), presymptomatic DMD ($P < 0.001$) (*Figure 1D*), LGMD2A ($P = 0.004$) and Becker ($P = 0.004$) and symptomatic DMD ($P < 0.001$) (*Figure 1E*). These analyses show a previously unreported common decrease in *RYR1* mRNA levels in human myopathies.

Ryanodine receptor type 1 protein is decreased in human non-RYR1-related myopathies

To investigate whether RyR1 protein levels are altered in human non-*RYR1*-RMs, we measured RyR1 protein content in muscle samples of patients suffering from IM (IBM and dermatomyositis included) and MM. Our results showed a significant decrease in RyR1 protein levels in both IM ($P < 0.001$) and MM ($P < 0.001$) muscle samples as compared with age-matched healthy control muscles (whether normalized by myosin content or total protein), with no significant modifications of the levels of the RyR1 channel stabilizer FKBP12 (*Figure 2A*). We observed a significant decrease of the sarco/endoplasmic reticulum Ca^{2+}-ATPase (SERCA) isoform 2 protein levels in both IM and MM samples, but no modifications of SERCA1 (*Figure S1A*). Both IM and MM muscle biopsies showed increased alpha-tubulin protein ($P = 0.013$) (*Figure S1A*), suggesting altered cytoskeleton. We performed a proteomic analysis to compare the molecular pathways altered in IM and MM muscle samples. Compared with control samples, IM and MM myopathies showed (1) decreased levels of proteins involved in muscle contraction, carbohydrate metabolism and mitochondrial function (*Figure 2B*) (with no significant alterations of Tom20 and oxidative phosphorylation complex proteins investigated by western blot; *Figure S1B*) and (2) increased levels of proteins found in the extracellular and the ER compartments, and in immune response (*Figure 2C*). Taken together, our results showed that two non-*RYR1*-RMs, IM and MM, have decreased RyR1 protein levels and share similar proteome alterations concerning muscle contraction, the extracellular and ER compartments, as well as metabolic pathways.

Ryanodine receptor type 1 protein depletion in vitro recapitulates the proteome changes observed in human non-RYR1-related myopathies

To investigate the specific role of RyR1 protein levels in myopathies, we performed RyR1 depletion in C2C12 mouse myoblasts. Myoblast differentiation was induced the day after siRNA transfection. We tested different doses of siRNAs and observed that the smallest applied dose (10 nM) was already effective to deplete RyR1 protein levels at Day 4 of transfection and Day 3 of differentiation (D4TD3D) and this effect was maintained until Day 7 of transfection and Day 6 of differentiation (D7TD6D) without any alterations of FKBP12 (*Figure 3A*). RyR1 depletion in myoblasts was associated with a transient increase in IP3R protein content at D4TD3D that was normalized at D7TD6D (*Figure 3A*). High (50 and 100 nM) but not small (10 nM) doses of siRNAs triggered an increase of SERCA1 protein (*Figure 3A*). Importantly, all doses of siRNAs induced increase of alpha-tubulin protein levels as observed in human IM and MM muscles at both D5TD3D and D7TD6D and of acetyl-tubulin protein levels at D4TD3D (*Figure 3A*). To avoid confounding effects, we used the lowest dose of siRNAs (10 nM) at D7TD6D for further analysis. RyR1 knockdown in myoblasts leads to non-aligned and disorganized myotubes with highly heterogenous size, strikingly different from control myotubes (*Figure S2A*). Proteomic analysis per-

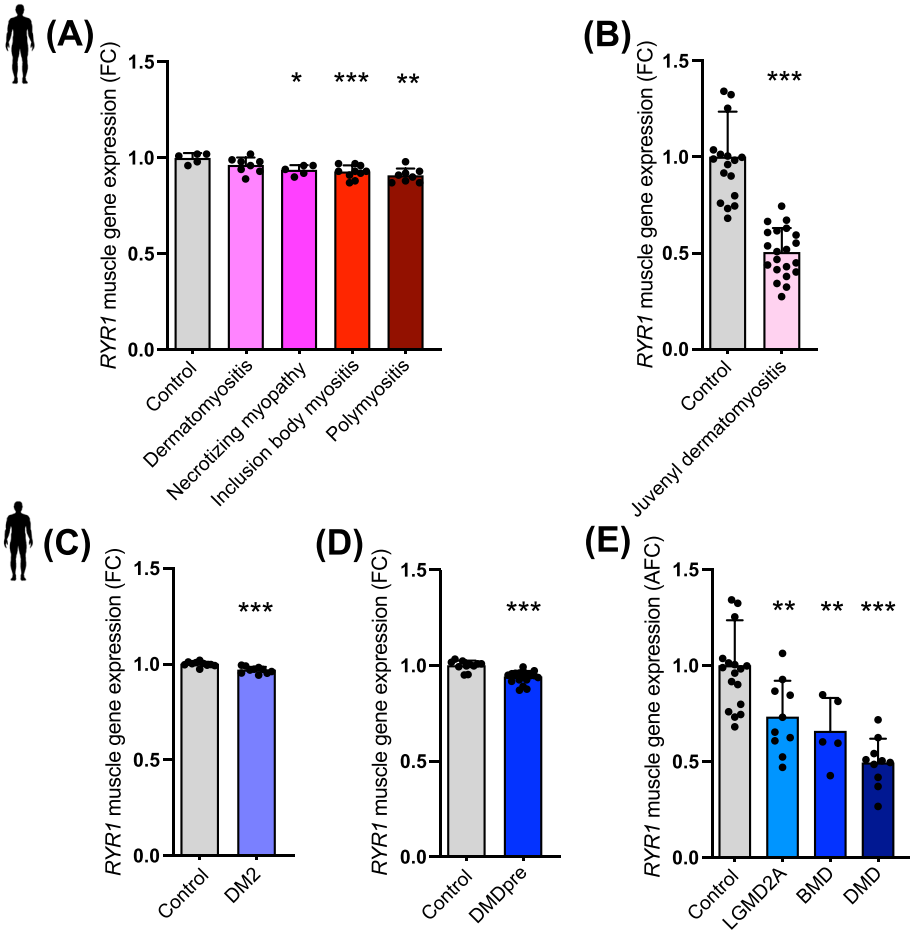

Figure 1 Skeletal muscle *RYR1* transcripts abundance is decreased in human myopathies. *RYR1* transcripts abundance in muscle from patients affected with (A) dermatomyositis (n = 8), necrotizing myopathy (n = 5), inclusion body myositis (n = 10) and polymyositis (n = 8) compared with healthy controls (n = 5) (GSE39454 dataset), one-way ANOVA followed by Dunnett's multiple-comparisons test; (B) juvenile dermatomyositis (n = 21) relative to healthy controls (n = 18) (E-GEOD-3307 dataset), Student's two-tailed t-test; (C) myotonic dystrophy 2 (DM2) (n = 10) relative to healthy controls (n = 10) (GSE37084 dataset), Student's two-tailed t-test; (D) Duchenne muscular dystrophy (DMD) (n = 23) compared with healthy controls (n = 14) (GSE6011 dataset), Student's two-tailed t-test; and (E) limb-girdle muscular dystrophy type 2A (LGMD2A) (n = 10), Becker muscular dystrophy (BMD) (n = 5) and DMD (n = 10) compared with relative healthy controls (n = 18) (E-GEOD-3307 dataset), one-way ANOVA followed by Dunnett's multiple-comparisons test. All data are shown as mean ± SD. $^{*}P \leq 0.05$, $^{**}P \leq 0.01$ and $^{***}P \leq 0.001$.

formed at D7TD6D showed more than 1000 significantly modified proteins, out of 4000 proteins identified (*Figure 3B*). RyR1 knockdown recapitulated the main alterations observed in human IM and MM by proteomics: (1) decreased muscle contraction proteins and energy metabolism proteins (*Figure 3C*) and (2) increased extracellular and ER compartments proteins and mitochondrial proteins (*Figure 3D*), suggesting a broader role of RyR1 in muscle health.

We tested whether RyR1 depletion in myoblasts may have led to the observed phenotype by altering the differentiation process. Using a wound healing assay, we observed an increase in myoblast migration in si-RyR1 cells at 12 h after the wound, which was similar with si-CTRL cells at 24 h post wound (*Figure S2B*). The key myogenic factors MyoD and Myogenin were not significantly modified at the mRNA level (*Figure S2C*) and Myogenin protein levels were unchanged (*Figure S2D*). However, si-RyR1 myotubes were hyperfused and showed nuclei aggregation with a higher number of nuclei per myotube (*Figure S2E*). Our proteomic data showed an increase in many myoblast fusion proteins, including the recently discovered muscle-specific fusion proteins Myomaker and Myomixer[27] (*Figure S2E*). To exclude a possible contribution of the alteration in myoblast differentiation to the observed phenotype, we next depleted RyR1 in differentiated myotubes. While the myotubes were homogenous and well organized before RyR1 depletion, they became heterogenous and mostly larger and showed a similar phenotype of aggregated nuclei at Day 9 of differentiation and Day 4 of transfection (D9DD4T; *Figure S2F*). These data suggest a specific myoblast hyperfusion and disorganized nuclei induced by RyR1 depletion. We then performed further analyses on the myotubes resulting from RyR1 depletion in myoblasts, to

DOI: 10.1002/jcsm.13349

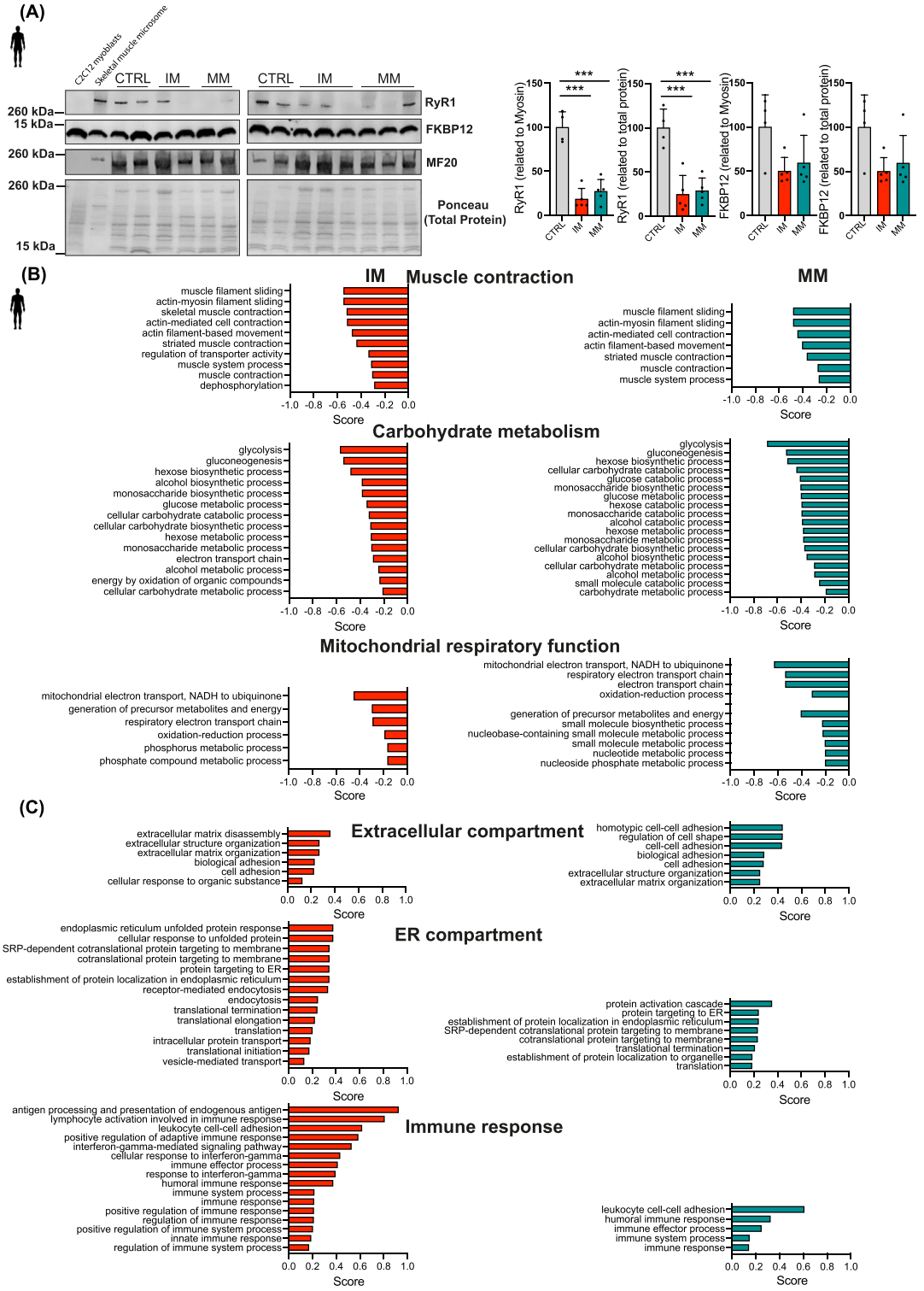

Figure 2 Non-*RYR1*-related myopathies show decreased RyR1 protein content, with similar proteomics identified alterations. (A) Representative immunoblots and quantifications of RyR1, FKBP12 and myosin (MF20) proteins in inflammatory myopathy (IM) (n = 5) and mitochondrial myopathy (MM) (n = 5) compared with healthy controls (n = 4) related to myosin (MF20) or total protein, one-way ANOVA followed by Dunnett's multiple-comparisons test. (B) Proteomic analysis of protein groups related to Gene Ontology Biological Processes (GoBP) that are significantly decreased in IM (n = 4) and MM (n = 4) as compared with healthy controls (n = 4). (C) Proteomic analysis of protein groups related to GoBP that are significantly increased in IM (n = 4) and MM (n = 4) as compared with healthy controls (n = 4). Benjamini–Hochberg's corrected t-test. Data in A are shown as mean ± SD. ***$P \leq 0.001$.

DOI: 10.1002/jcsm.13349

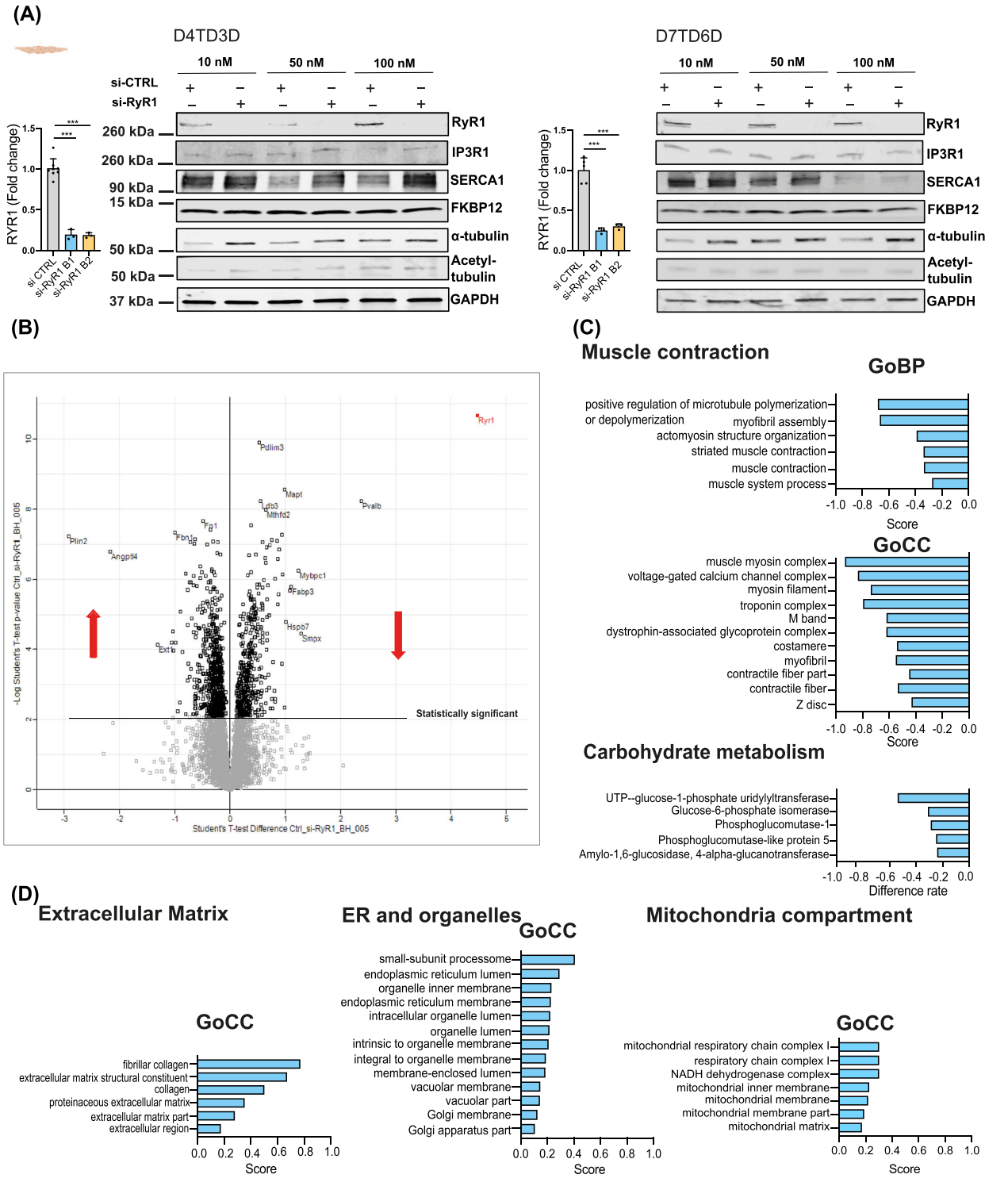

Figure 3 RyR1 protein depletion in myoblasts leads to myotubes with proteomics alterations similar to those observed in human myopathies. (A) Transcripts of RyR1 and immunoblots of RyR1, IP3R1, SERCA1, FKBP12, alpha-tubulin, acetylated tubulin and GAPDH at Day 4 of transfection and Day 3 of differentiation (D4TD3D) and Day 7 of transfection and Day 6 of differentiation (D7TD6D). (B) Volcano plot of proteomic analysis showing the proteins significantly altered in si-RyR1 compared with si-CTRL myotubes. (C) Proteomic analysis of protein groups related to Gene Ontology Biological Processes (GoBP) and Cellular Component (GoCC) that are significantly downregulated in si-RyR1 compared with si-CTRL myotubes (n = 6 independent biological replicates per group, Benjamini–Hochberg's corrected t-test). (D) Proteomic analysis of protein groups related to GoBP and GoCC that are significantly upregulated in si-RyR1 compared with si-CTRL myotubes (n = 6 independent biological replicates per group, Benjamini–Hochberg's corrected t-test).

better characterize their phenotype (*Figure S3A*). Glucose transporter 4 (GLUT4) transcripts were increased in si-RyR1 at D4TD3D (*Figure S3B*). Transcript levels of myosin heavy chain and of genes involved in oxidative stress were not different at D4TD3D but were all significantly decreased at D7TD6D (*Figure S3C*).

Together, our results show that RyR1 protein depletion in vitro in myoblasts, with no changes in SERCA or IP3R protein levels, does not delay muscle differentiation but induces anarchic myoblast hyperfusion, leading to disorganized myotubes, and recapitulates most of the changes in molecular pathways observed in human non-*RYR1*-RMs, including changes in muscle contraction proteins, energy metabolism proteins and ER compartments proteins.

Ryanodine receptor type 1 protein depletion induces defects in endoplasmic reticulum–mitochondria contact and mitophagy gene expression and results in mitochondrial aggregation

Our proteomics data showed an increase in mitochondrial specific proteins, and western blot showed increased mitochondrial protein Tom20 levels in si-RyR1 myotubes (*Figure 4A*). Immunofluorescence showed mitochondrial (Tom20) aggregation in some regions of the si-RyR1 myotubes, around clustered nuclei, suggesting altered mitochondrial distribution (*Figure 4B*). We then used transmission electron microscopy (TEM) to investigate mitochondrial morphology and subcellular distribution. Elongated mitochondria accumulated in si-RyR1 cells (*Figure 4C*). The number of mitochondria per field was increased in si-RyR1 myotubes ($P = 0.005$), associated to a significant decrease in mitochondrial circularity ($P = 0.016$) (*Figure 4C*). These elongated mitochondria appeared darker with opaque matrix. Elongated mitochondria have been shown to be spared from degradation,[28] suggesting a defect in mitophagy in si-RyR1 cells. As ER plays an important role in mitochondrial dynamics,[29] we measured ER–mitochondria contacts. ER–mitochondria contact length was reduced in si-RyR1 myotubes ($P < 0.001$), without any alterations in the distance between the organelles (*Figure 4C*). Transcript levels of PARK2 were significantly decreased ($P = 0.037$) with no significant changes in those of PINK1 and BNIP3 (*Figure 4D*). We observed no alterations of the transcript levels of the classical autophagy genes sequestosome 1 and Beclin1 (*Figure 4E*), but the autophagy marker light chain 3 (LC3) protein forms I and II were both increased in si-RyR1 cells (*Figure S3D*) as previously reported in RyR1-Rec muscles.[25] Importantly, a decrease in PARK2 has been shown to completely impair mitophagy in muscle,[17] as we have recently shown in DMD.[30] We analysed RyR1-Rec mouse muscles that showed a 50% decrease of RyR1 protein levels upon tamoxifen injection, without any alterations of FKBP12 (*Figure 4E*) as previously reported,[25] and observed a significant increase of the optical atrophy 1 (OPA1) protein levels, supporting elongated mitochondria in RyR1-Rec muscles (*Figure 4F*). Together, our results show that RyR1 protein depletion impairs ER–mitochondria tethering and induces accumulation of elongated mitochondria, potentially through defects in mitophagy.

Ryanodine receptor type 1 protein depletion alters endoplasmic reticulum–mitochondria Ca^{2+} transfer and mitochondrial function

We investigated whether the decrease in ER–mitochondria contact length in si-RyR1 may affect Ca^{2+} transfer from the ER to the mitochondria. We first investigated Ca^{2+} release from the ER using Fluo-4/AM and caffeine stimulation to open the RyR1 and observed that caffeine-induced ER Ca^{2+} release was blunted in si-RyR1 cells ($P = 0.021$) (*Figure 5A*). However, si-RyR1 cells elicited ER Ca^{2+} transients in response to thapsigargin stimulation, which were much lower in si-CTRL cells that previously responded to the caffeine stimulation (*Figure 5A*), suggesting preserved ER Ca^{2+} stores in si-RyR1 cells. We then investigated ER–mitochondria Ca^{2+} transfer using Rhod-2/AM and thapsigargin stimulation in the presence of dantrolene (to inhibit the RyR1 channel) to avoid any input of Ca^{2+} from RyR1 channels. Mitochondrial Ca^{2+} uptake was blunted in si-RyR1 myotubes ($P = 0.033$) (*Figure 5B*), indicating that the reduction in ER–mitochondria contact length might be sufficient to alter Ca^{2+} transfer from the ER to the mitochondria in si-RyR1 myotubes.

We next investigated mitochondrial function with high-resolution respirometry. Using two different si-RyR1, we observed a significant decrease in leak respiration (MP_L) ($P < 0.01$) and maximal respiration capacity ($P < 0.05$) in si-RyR1 compared with si-CTRL myotubes (*Figure 5C*). Our results showed a significant increase in the contribution of succinate-linked pathway to the maximal respiration especially in the non-phosphorylated state, despite the overall decrease in maximal respiration capacity in si-RyR1 myotubes (*Figure 5D*), suggesting a higher lipid oxidation capacity in si-RyR1 cells.

As ER–mitochondria Ca^{2+} transfer plays a key role in the regulation of numerous mitochondrial functions including ATP production and cell death,[31] we measured the phosphorylation levels of pyruvate dehydrogenase (PDH), as a readout of mitochondrial Ca^{2+} uptake.[2] PDH phosphorylation levels on Serine^{293} (P PDH E1 Ser^{293}) were significantly increased in RyR1-Rec muscles ($P < 0.001$) (*Figure 5E*) and in both human IM ($P = 0.007$) and MM ($P = 0.042$) (*Figure 5F*), suggesting a defect in mitochondrial Ca^{2+} uptake and PDH activation, which could contribute to impaired mitochondrial function.

Together, our results show that RyR1 protein depletion impairs mitochondrial Ca^{2+} uptake and mitochondrial function, likely by altering ER–mitochondria tethering.

DOI: 10.1002/jcsm.13349

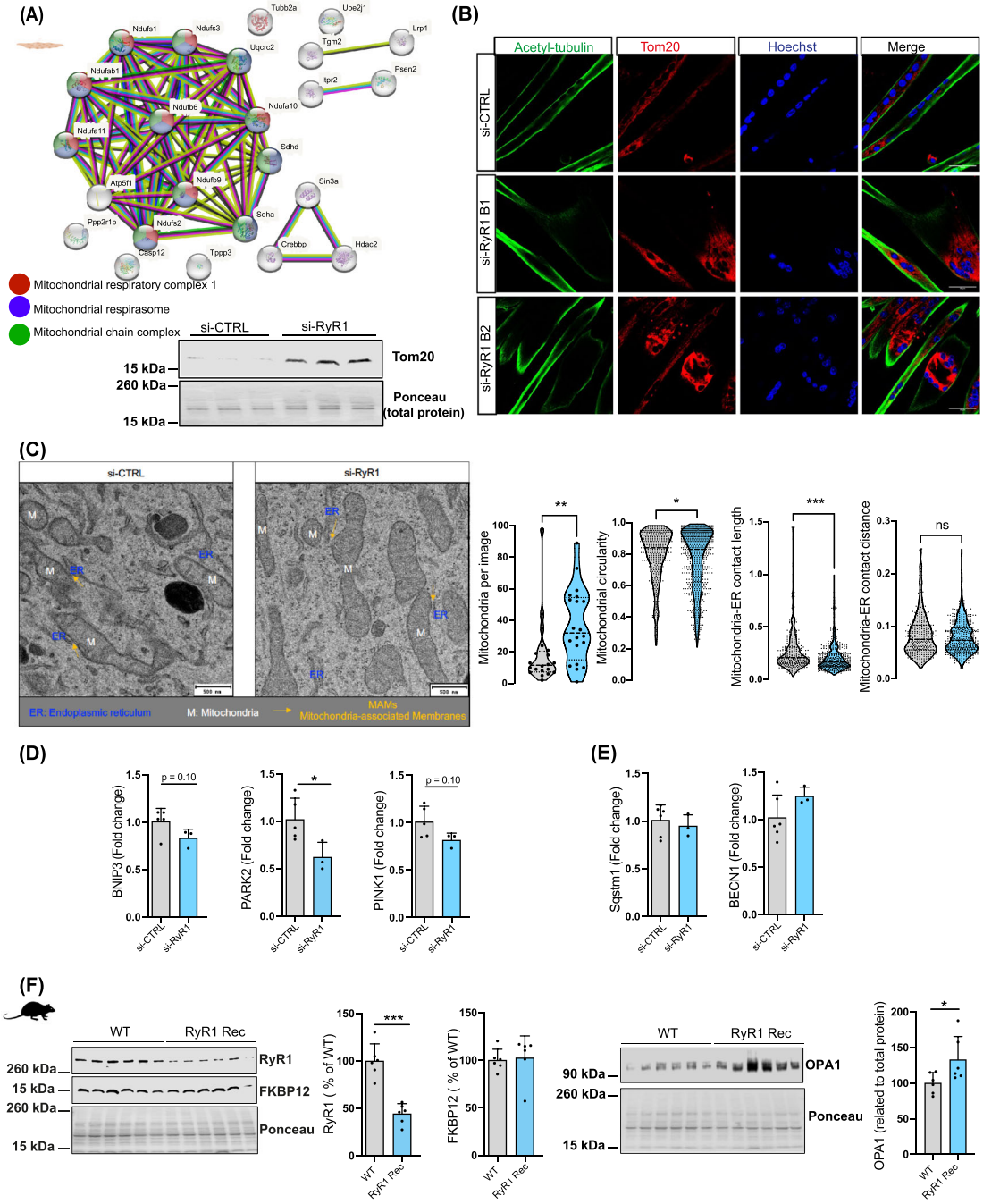

Figure 4 RyR1 knockdown myotubes accumulate elongated mitochondria and show a reduction of endoplasmic reticulum (ER)–mitochondria contact and mitophagy gene expression. (A) STRING protein–protein interaction network of mitochondrial proteins significantly increased in C2C12 si-RyR1 compared with si-CTRL myotubes at Day 7 of transfection and Day 6 of differentiation (D7TD6D) from the proteomics data, and western blot showing increase of the mitochondrial outer membrane protein, Tom20, in si-RyR1 myotubes compared with si-CTRL myotubes at D7TD6D. (B) Representative confocal images of acetylated tubulin and Tom20 immunofluorescence staining in C2C12 cells transfected with two different siRNAs against RyR1 (B1 and B2) and compared with si-CTRL at D7TD6D. Hoechst 33342 was used to stain the nuclei (n = 3 independent biological replicates). Magnification: ×40. Scale bar: 50 μM. (C) Representative transmission electron microscopy (TEM) images of si-CTRL and si-RyR1 myotubes at D7TD6D, and quantifications of the number of mitochondria counted per image and mitochondrial circularity (371 mitochondria counted in si-CTRL and 741 in si-RyR1 from n = 2 independent biological replicates, Kolmogorov–Smirnov's test), mitochondria–ER length (μm) and distance (μm) (309 contacts counted in si-CTRL and 457 in si-RyR1 from n = 2 independent biological replicates, Kolmogorov–Smirnov's test). (D, E) mRNA levels of genes involved in mitophagy (D) and autophagy (E) in si-CTRL and si-RyR1 myotubes (n = 6 and 3 independent biological replicates, respectively, Student's two-tailed t-test). (F) RyR1, FKBP12 and OPA1 immunoblots in RyR1-Rec mouse muscles at Day 75 after tamoxifen injection compared with wild-type mouse muscles and their quantifications (mean of two technical replicates, n = 6 mice per group). Data are shown as mean ± SD. $^{*}P \leq 0.05$, $^{**}P \leq 0.01$ and $^{***}P \leq 0.001$.

DOI: 10.1002/jcsm.13349

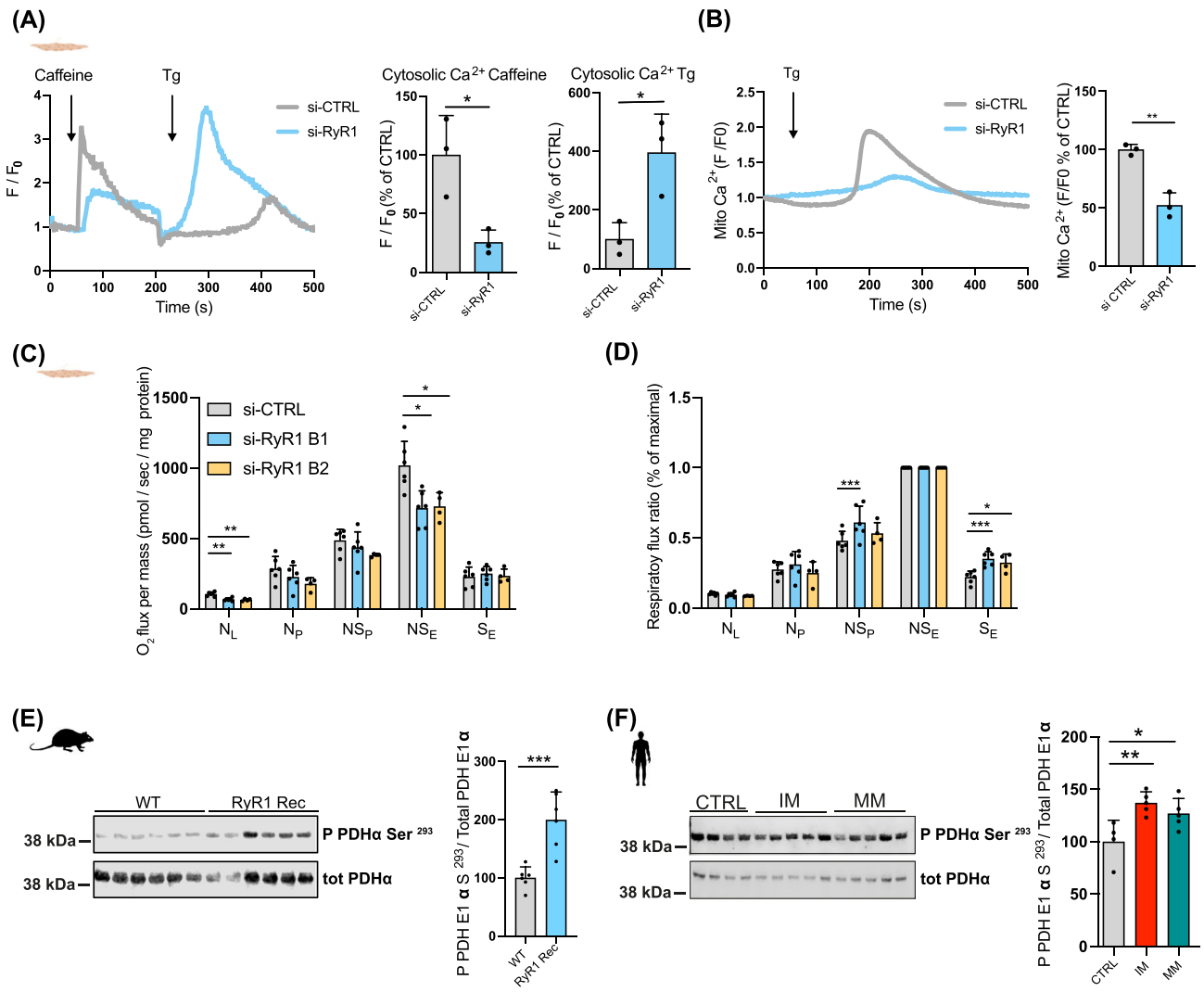

Figure 5 RyR1 protein reduction impairs mitochondrial Ca^{2+} uptake and mitochondrial function. (A) Normalized Fluo-4 fluorescence traces and quantification of caffeine and thapsigargin-related sarcoplasmic reticulum (SR) Ca^{2+} release in C2C12 si-CTRL and si-RyR1 myotubes at Day 7 of transfection and Day 6 of differentiation (D7TD6D) (n = 3 independent biological replicates per group, Student's two-tailed t-test). (B) Normalized Rhod-2 fluorescence traces and quantification of mitochondrial Ca^{2+} uptake in si-CTRL and si-RyR1 myotubes pre-treated with 10 μM of dantrolene (n = 3 independent biological replicates per group, Student's two-tailed t-test). (C) O_2 flux per mass (pmol/s/mg of protein) in si-CTRL and si-RyR1 myotubes at D7TD6D. MP_L, malate pyruvate leak state; N_P, N-linked OXPHOS state with ADP-stimulated; NS_P, N- and S-OXPHOS pathways; NS_E, ET state, noncoupled and S_E, S-pathway. (D) Respiratory flux ratio si-CTRL (n = 5 independent biological replicates) and si-RyR1 myotubes (n = 6 si-RyR1 Batch 1 [B1] and n = 4 si-RyR1 Batch 2 [B2] independent biological replicates), one-way ANOVA with Dunnett's multiple-comparisons test. (E) Immunoblots and quantifications of phosphorylated PDH E1α at Serine^{293} related to total PDH E1α in RyR1-Rec versus wild-type mouse muscles (mean of two technical replicates, n = 6 mice per group), Student's two-tailed t-test. (E) Immunoblots and quantifications of phosphorylated PDH E1α at Serine^{293} related to total PDH E1α in human suffering from inflammatory myopathy (IM) (n = 5) and mitochondrial myopathy (MM) (n = 5) compared with control healthy muscles (n = 4). Mean of two technical replicates, one-way ANOVA followed by Dunnett's multiple-comparisons tests. All data are shown as mean ± SD. $^*P \leq 0.05$, $^{**}P \leq 0.01$ and $^{***}P \leq 0.001$.

Ryanodine receptor type 1 depleted myotubes show accumulation of sphingolipids, phospholipids and glycerolipids

Our data suggest higher lipid oxidation rates in si-RyR1 myotubes. Our proteomics data showed upregulation of proteins related to lipid metabolism in si-RyR1 myotubes (*Figure 6A*), with the top modified being the LD coating protein perilipin 2 (Plin2) (*Figure 6B*), with an inverse association between RyR1 and Plin2 (*Figure 6C*), which we confirmed by western blot (*Figure 6D*). Plin2 protein levels were not significantly different in RyR1-Rec mouse muscles (*Figure 6D*), in differentiated myotubes transfected with si-RyR1 (neither LD amount; *Figure S4A*) or in human IM muscles but tended to increase in human MM muscles (*Figure 6D*), suggesting that RyR1 depletion associated with Plin2 protein alterations may depend on

DOI: 10.1002/jcsm.13349

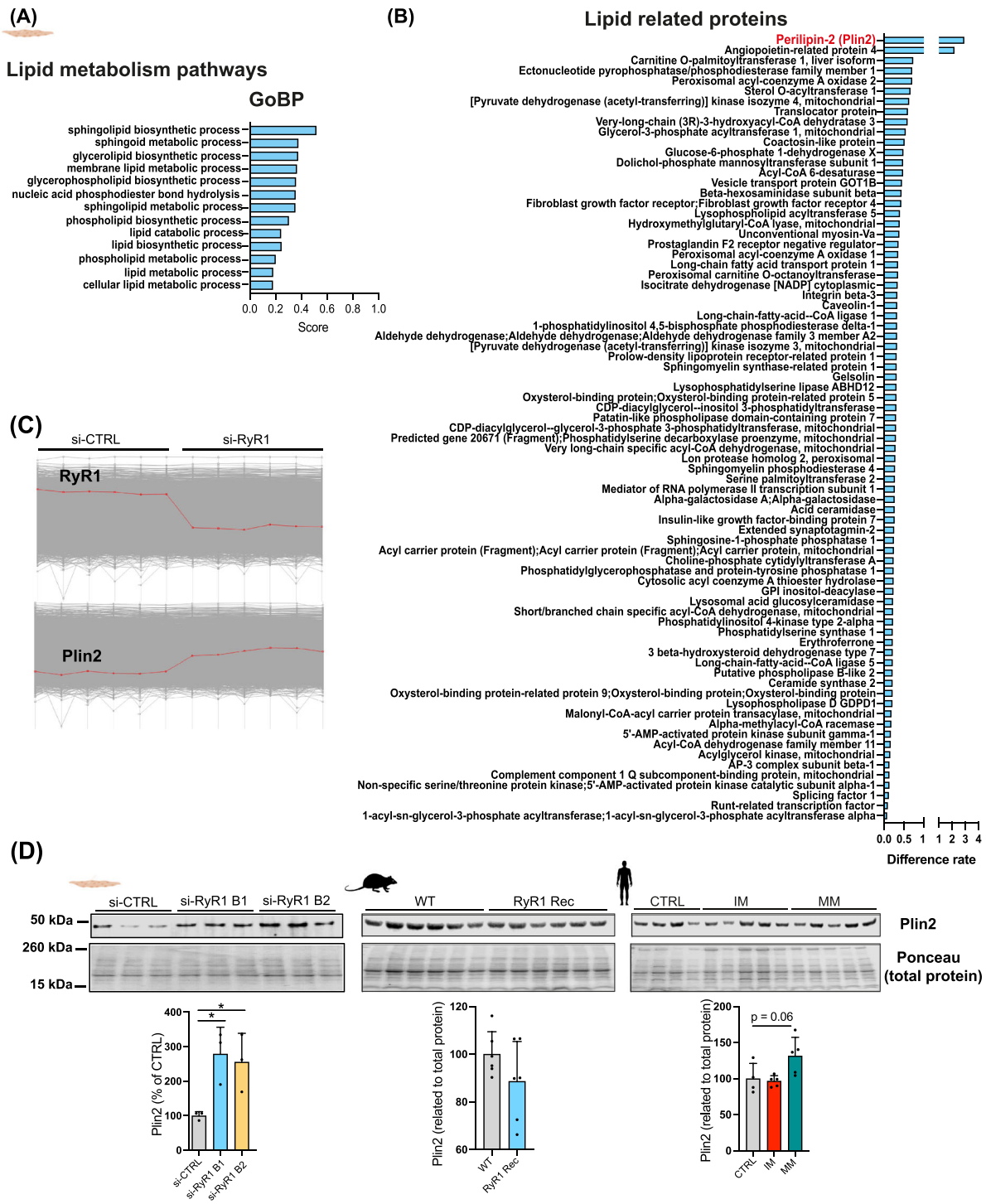

Figure 6 RyR1 protein depletion induces upregulation of lipid-related proteins. (A) Proteomic analysis showing protein groups related to Gene Ontology Biological Processes (GoBP) involved in lipid metabolism that are significantly upregulated in si-RyR1 compared with si-CTRL myotubes. Benjamini–Hochberg's corrected *t*-test. (B) List of proteins involved in lipid homeostasis that are significantly upregulated in si-RyR1 compared with si-CTRL myotubes. (C) Scheme of RyR1 and perilipin 2 (Plin2) inverse association in si-CTRL and si-RyR1 from proteomic data. (D) Representative immunoblots of Plin2 protein in si-CTRL and si-RyR1 (B1 and B2) myotubes at Day 7 of transfection and Day 6 of differentiation (D7TD6D) and quantifications of Plin2 related to total protein (n = 3 independent biological replicates per group, one-way ANOVA followed by Dunnett's multiple-comparisons tests); in RyR1-Rec versus wild-type (WT) mouse muscles (mean of two technical replicates, n = 6 mice per group), Student's two-tailed *t*-test; and in human suffering from inflammatory myopathy (IM) (n = 5) and mitochondrial myopathy (MM) (n = 5) compared with control healthy muscles (n = 4) (mean of two technical replicates, one-way ANOVA followed by Dunnett's multiple-comparisons tests). Data in (D) are shown as mean ± SD. $^*P \leq 0.05$.

DOI: 10.1002/jcsm.13349

the levels and/or timing of RyR1 depletion. RyR1 depletion in myoblasts led to an accumulation of LDs, stained by three different probes (Bodipy, Nile Red and LipiDye II) (*Figure 7A*), supporting the increased Plin2 protein. Semi-quantitative lipidomic analysis showed a large increase in the proportion of sphingolipids, including the deleterious ceramides and dihydroceramides species we recently reported in DMD muscles[32] (*Figure 7B*), phospholipids (*Figure 7C*) and many

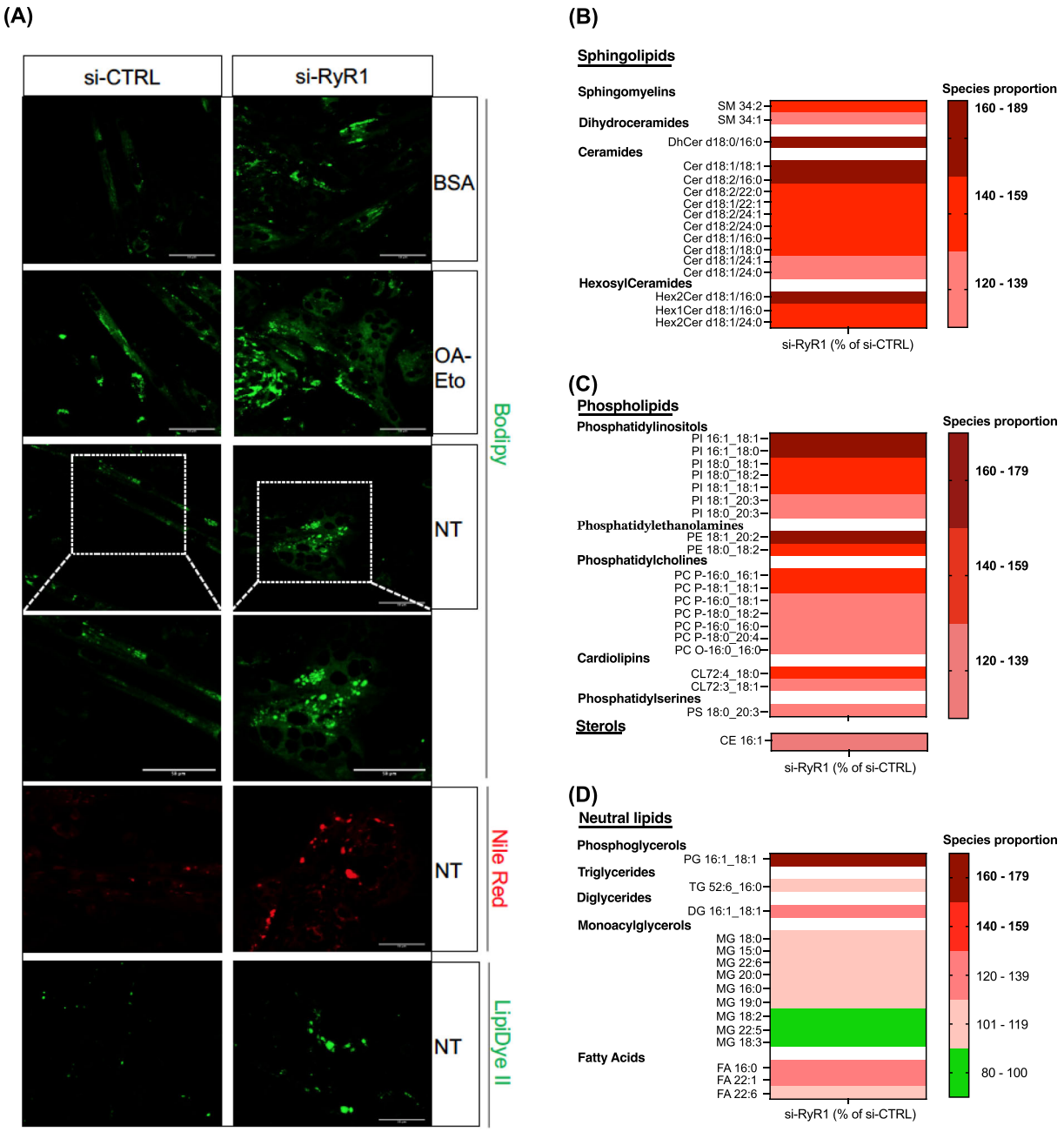

Figure 7 RyR1 protein depletion leads to deleterious lipid species accumulation. (A) Representative confocal images of lipid droplets (LDs) amount using Bodipy 493/503 and double checked using Nile Red and LipiDye II stainings in si-CTRL and si-RyR1 myotubes at Day 7 of transfection and Day 6 of differentiation (D7DD6T), from *n* = 6 independent biological replicates. C2C12 myotubes treated for 24 h with 3% bovine serum albumin (BSA) or a combination of oleic acid (200 μM) and etomoxir (1 mM) (OA-Eto) were used as negative and positive controls for LDs staining, respectively. Magnification: ×40. Scale bar: 50 μm. (B–D) Lipidomic analysis of si-CTRL and si-RyR1 myotubes at D7TD6D (6 technical replicates from *n* = 2 independent biological replicates). Lipid species were expressed as a proportion of total species detected. Only the lipid species that showed changes in both independent biological replicates were considered as altered. Data are expressed as percentage of si-CTRL.

neutral lipid species (*Figure 7D*) in si-RyR1, demonstrating that RyR1 protein depletion in myoblasts triggers major alterations of lipid homeostasis in the resulting myotubes.

Ryanodine receptor type 1 protein decrease induces endoplasmic reticulum stress in cultured cells, mouse and human muscle samples

How RyR1 protein reduction mediates muscular disorders is unknown. We hypothesized that RyR1 protein reduction may induce ER stress and cause defects in lipid metabolism, ER–mitochondria Ca^{2+} transfer, mitophagy and mitochondrial function. In line with this hypothesis, the ER stress marker GRP78-Bip (P = 0.047) and CHOP-DDIT3 protein levels ($P < 0.001$) were increased in si-RyR1 myotubes (*Figure 8A*). However, we did not observe significant changes in the levels of phosphorylated eIF2α as both phospho-eIF2α and total eIF2α were increased (*Figure 8A*). The increase in GRP78-Bip protein levels with no significant modifications in the phosphorylation levels of eIF2α was also observed when RyR1 was depleted after myotube differentiation (*Figure S4B*). Interestingly, RyR1-Rec muscles showed increased GRP78-Bip (P = 0.001) and CHOP-DDIT3 (P = 0.009) protein levels as observed in our cellular models, associated with decreased eIF2α phosphorylation levels (P = 0.035) (*Figure 8B*). An increase in GRP78-Bip and CHOP-DDIT3 proteins was also observed in our human IM and MM muscles (*Figure 8C*). Bioinformatic analysis showed increased transcript levels of ER stress markers in various human IM (IBM, dermatomyosis, necrotizing myositis) and muscular dystrophies (BMD, DMD and LGMD2A) showing reduced *RYR1* transcript levels (*Figure 8D*). ER stress markers negatively correlated with *RYR1* transcript levels in control population (*Figure 8E*). Taken together, our data show that (1) RyR1 depletion leads to ER stress in muscle cells independently of the differentiation stage and in vivo in a mouse model of RyR1 depletion in mature myofibers, that (2) there is an association between decreased RyR1 transcript/protein levels and increased ER stress markers in human muscle and that (3) there is a negative correlation between *RYR1* transcript levels and ER stress markers in muscle from non-diseased population.

Discussion

We highlight a previously unreported significant decrease of *RYR1* transcripts in various myopathies. This systematic decrease in *RYR1* transcripts in myopathies either reflects muscle remodelling or highlights its potential role in the pathophysiology of muscle disease, in addition to potentially constitute a new diagnosis tool for myopathies. The unsolved question is how *RYR1* transcripts are affected during myopathies, calling for future investigations. A role of calpain-activated protein degradation in RyR1 protein decrease in IBM has been previously suggested.[8] We here confirm in different IM forms (including dermatomyositis and IBM) a systematic decrease in RyR1 protein content. While proteolysis might potentially explain decreased RyR1 protein content in myopathies, it might not be the only mechanism involved as we have observed decreased *RYR1* transcript levels at earlier and presymptomatic stages of DMD. We have also recently reported sphingolipid accumulation in presymptomatic DMD muscle samples[32] and in sarcopenia.[33] Interestingly, we here show sphingolipid accumulation in myotubes resulting from RyR1 depletion myoblasts.

Our results show for the first time an increase in GRP78-Bip and CHOP in si-RyR1 myotubes, and in RyR1-Rec mouse muscles as well as in human IM and MM muscles showing decreased RyR1 protein levels, indicating an activation of ER stress and its pro-apoptotic effector in response to RyR1 protein decrease. We detected a negative association between ER stress markers and muscle *RYR1* content in various myopathies. Of note, transcripts of the kinase activating the pro-survival factor eIF2α, eIF2AK3/PERK, are also increased in human myopathies and negatively correlate with *RYR1* levels (*Figure 6D*). eIF2α kinases have been shown to increase in response to decreased eIF2α phosphorylation as an attempt to rescue cell survival. However, this adaptive mechanism is rarely successful.[14] Reduced eIF2α phosphorylation has been associated with increased CHOP and eIF2α kinase protein levels, but not with their activity, in aged muscles.[34] ER stress-mediated apoptosis has been implicated in the pathogenesis of several diseases.[35] A recent study has reported ER stress in a mouse model of I4898T *RYR1* mutation, the most studied mutation on the *RYR1* gene, with a UPR response essentially mediated by CHOP.[10] Accordingly, the deletion of the gene encoding CHOP preserves tissue function in case of chronic ER stress/maladaptive UPR.[36]

RyR1 protein depletion may trigger ER stress to induce muscular disorders, but ER stress may also be secondary to other disorders induced by RyR1 protein depletion. Indeed, it is well established that accumulation of misfolded proteins, excessive numbers of damaged lipids or Ca^{2+} imbalance can induce ER stress.[11,37] Despite the impairment of ER–mitochondria Ca^{2+} transfer in si-RyR1 myotubes, our investigations did not reveal significant alterations of ER Ca^{2+} content in si-RyR1 myotubes that could trigger ER stress. The ER is an important site of lipid metabolism.[38] Due to its key position at the ER membrane, the RyR1 might play a direct or indirect role in lipid synthesis/metabolism and/or modulate the ER structure and function in another manner. However, RyR1 depletion in differentiated myotubes led to ER stress without marked lipid accumulation in myotubes, contrary to what was observed after RyR1 depletion in myoblasts. RyR1-Rec mouse muscles did not show increased Plin2

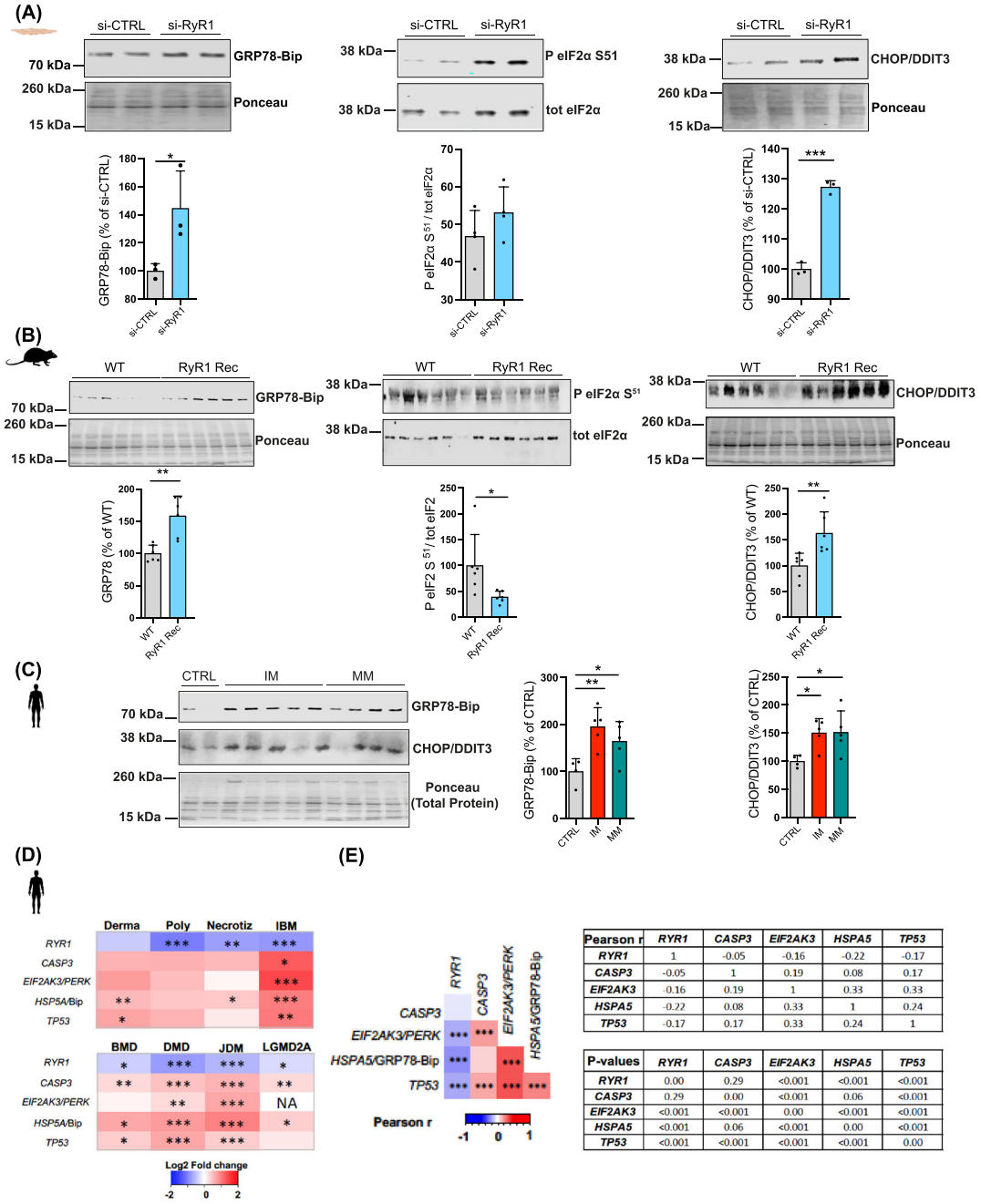

Pearson r	RYR1	CASP3	EIF2AK3	HSPA5	TP53
RYR1	1	-0.05	-0.16	-0.22	-0.17
CASP3	-0.05	1	0.19	0.08	0.17
EIF2AK3	-0.16	0.19	1	0.33	0.33
HSPA5	-0.22	0.08	0.33	1	0.24
TP53	-0.17	0.17	0.33	0.24	1

P-values	RYR1	CASP3	EIF2AK3	HSPA5	TP53
RYR1	0.00	0.29	<0.001	<0.001	<0.001
CASP3	0.29	0.00	<0.001	0.06	<0.001
EIF2AK3	<0.001	<0.001	0.00	<0.001	<0.001
HSPA5	<0.001	0.06	<0.001	0.00	<0.001
TP53	<0.001	<0.001	<0.001	<0.001	0.00

Figure 8 RyR1 levels inversely correlate with endoplasmic reticulum (ER) stress in muscle cells, mouse muscle and human myopathies. (A) Representative immunoblots and quantifications of GRP78-Bip, eIF2α phospho-S51, total eIF2α protein levels, and CHOP-DDIT3, in C2C12 si-CTRL and si-RyR1 myotubes at Day 7 of transfection and Day 6 of differentiation (D7TD6D), related to total protein (n = 3–4 independent biological replicates per group, Student's two-tailed t-test). (B) Representative immunoblots and quantifications of GRP78-Bip, eIF2α phospho-S51, total eIF2α and CHOP-DDIT3 protein levels related to total protein in wild-type (WT) and RyR1-Rec mouse muscles (mean of four technical replicates, n = 6 mice per group, Student's two-tailed t-test). (C) Representative immunoblots and quantifications of GRP78-Bip and CHOP-DDIT3 protein levels related to total protein in human muscles biopsies from inflammatory myopathy (IM) (n = 5) and mitochondrial myopathy (MM) (n = 5) compared with control healthy subjects (n = 4); mean of at least two technical replicates; one-way ANOVA followed by Dunnett's multiple-comparisons tests. (D) Heat map of *RYR1* and ER stress transcripts in IMs and dystrophies (dermatomyositis [Derma], n = 8; polymyositis [Poly], n = 8; necrotizing myopathy [Necrotiz], n = 5; inclusion body myositis [IBM], n = 10; Becker muscular dystrophy [BMD], n = 5; Duchenne muscular dystrophy [DMD], n = 10; juvenile dermatomyositis [JMD], n = 21; limb-girdle muscular dystrophy 2A [LGMD2A], n = 10) from publicly available datasets (GSE39454 and E-GEOD-3307). (E) Correlogram showing Pearson's correlations between *RYR1* transcript levels and ER stress markers in post-mortem skeletal muscle biopsies from the Genotype-Tissue Expression (GTEx) v7 dataset (n = 491, Pearson's r and P-values included). Data in (A), (B) and (C) are shown as mean ± SD. $^{*}P \leq 0.05$, $^{**}P \leq 0.01$ and $^{***}P \leq 0.001$.

DOI: 10.1002/jcsm.13349

protein either, suggesting that ER stress in response to RyR1 depletion is not primarily induced by lipid accumulation. However, lipid accumulation could enhance RyR1 depletion-induced ER stress, suggesting a key role for RyR1 in the regulation of the ER network dynamics and lipid biosynthesis during myoblast differentiation. Further investigations are required to elucidate this.

A previous study showed an increase in LC3 (all forms) in RyR1-Rec muscles, suggesting defects in autophagy.[25] We also observed accumulation of all forms of LC3 in our si-RyR1 cells (*Figure S3D*). LC3 is well known as an autophagosome marker and can also be incorporated into protein aggregates independently of autophagy,[39] imposing caution while interpreting LC3 I and II simultaneous increase. Our results here suggest a defect in mitophagy in si-RyR1 cells, supported by a decreased length of ER–mitochondria contacts, decreased PARK2 levels and accumulation of elongated and non-functional mitochondria. Our findings however do not exclude a global defect in autophagy. As PARK2 promotes the recruitment of p62, which in turn is responsible for the recruitment of ubiquitinated cargo into autophagosomes by binding to LC3, we cannot exclude that PARK2 decrease might prevent the recruitment of p62 and its binding to LC3, resulting in the accumulation of LC3.

Taken together, our results point to a widespread decrease in RyR1 content in myopathies and establish a role of RyR1 protein decrease in the induction of ER stress, a mechanism associated with an increasing number of diseases including myopathies. Understanding the molecular mechanisms behind this might open rapidly implementable therapeutic approaches to alleviate the muscular disorders induced by decreased RyR1 content, as ER stress inhibitors are already used in clinics for other diseases.[40]

Acknowledgements

We thank Prof. Romano Regazzi and Prof. Dario Divani, directors of the Department of Biomedical Sciences, for their support, infrastructure availability and discussions, and Mr. Gilles Dubuis and Mr. Clément Lanfranchi for technical support. Special thanks to all the patients who provided their consent for the use of their muscle biopsy samples. We thank Prof. Isabelle Marty and Dr. Anne Petiot from the University of Grenoble for providing us with RyR1-Rec mouse muscles, Prof. Andrew Marks, Prof. Steven Reiken and Prof. Haikel Dridi from Columbia University for the RyR1 antibody and muscle microsomes, and Prof. Marlen Knobloch from the University of Lausanne for sharing with us the LipiDye II probe. We also thank the proteomics, metabolomics, TEM and the cellular imaging facility platforms of the University of Lausanne.

Funding information

This work was supported by the Swiss National Science Foundation (grant IZK0Z3_173941 to NZ and grant PRIMA PR00P3_193166 to ICL-M), the Subside Tremplin/Relève Académique to NZ and the University of Lausanne financial support to JV, BK, NP and NZ.

Conflict of interest statement

There are no competing interests.

Data availability statement

All data generated and analysed during this study are included in this published article (and its supporting information). The proteomics data generated in this study have been deposited with PRIDE under accession code PXD039693.

Online supplementary material

Additional supporting information may be found online in the Supporting Information section at the end of the article.

References

1. Marks AR, Tempst P, Hwang KS, Taubman MB, Inui M, Chadwick C, et al. Molecular cloning and characterization of the ryanodine receptor/junctional channel complex cDNA from skeletal muscle sarcoplasmic reticulum. *Proc Natl Acad Sci U S A* 1989;**86**:8683–8687.
2. Zanou N, Dridi H, Reiken S, Imamura de Lima T, Donnelly C, de Marchi U, et al. Acute RyR1 Ca^{2+} leak enhances NADH-linked mitochondrial respiratory capacity. *Nat Commun* 2021;**12**:7219.
3. Bellinger AM, Reiken S, Carlson C, Mongillo M, Liu X, Rothman L, et al. Hypernitrosylated ryanodine receptor calcium release channels are leaky in dystrophic muscle. *Nat Med* 2009;**15**:325–330.
4. Waning DL, Mohammad KS, Reiken S, Xie W, Andersson DC, John S, et al. Excess TGF-β mediates muscle weakness associated with bone metastases in mice. *Nat Med* 2015;**21**:1262–1271.
5. Andersson DC, Betzenhauser MJ, Reiken S, Meli AC, Umanskaya A, Xie W, et al. Ryanodine receptor oxidation causes intracellular calcium leak and muscle weakness in aging. *Cell Metab* 2011;**14**:196–207.
6. Clarke NF, Waddell LB, Cooper ST, Perry M, Smith RLL, Kornberg AJ, et al. Recessive mutations in RYR1 are a common cause

of congenital fiber type disproportion. *Hum Mutat* 2010;**31**:E1544–E1550.
7. Garibaldi M, Rendu J, Brocard J, Lacene E, Fauré J, Brochier G, et al. 'Dusty core disease' (DuCD): expanding morphological spectrum of RYR1 recessive myopathies. *Acta Neuropathol Commun* 2019;**7**:3.
8. Amici DR, Pinal-Fernandez I, Mázala DAG, Lloyd TE, Corse AM, Christopher-Stine L, et al. Calcium dysregulation, functional calpainopathy, and endoplasmic reticulum stress in sporadic inclusion body myositis. *Acta Neuropathol Commun* 2017;**5**:24.
9. Kawasaki N, Asada R, Saito A, Kanemoto S, Imaizumi K. Obesity-induced endoplasmic reticulum stress causes chronic inflammation in adipose tissue. *Sci Rep* 2012;**2**:799.
10. Germani S, Marchetti AC, Guidarelli A, Cantoni O, Sorrentino V, Zito E. Loss-of-rescue of Ryr1I4895T-related pathology by the genetic inhibition of the ER stress response mediator CHOP. *Sci Rep* 2022; **12**:20632.
11. Pauly M, Angebault-Prouteau C, Dridi H, Notarnicola C, Scheuermann V, Lacampagne A, et al. ER stress disturbs SR/ER-mitochondria Ca^{2+} transfer: implications in Duchenne muscular dystrophy. *Biochim Biophys Acta Mol Basis Dis* 2017; **1863**:2229–2239.
12. Malhi H, Kaufman RJ. Endoplasmic reticulum stress in liver disease. *J Hepatol* 2011; **54**:795–809.
13. Lee AS. The ER chaperone and signaling regulator GRP78/BiP as a monitor of endoplasmic reticulum stress. *Methods* 2005; **35**:373–381.
14. Rozpedek W, Pytel D, Mucha B, Leszczynska H, Diehl JA, Majsterek I. The role of the PERK/eIF2α/ATF4/CHOP signaling pathway in tumor progression during endoplasmic reticulum stress. *Curr Mol Med* 2016;**16**:533–544.
15. Raiborg C, Wenzel EM, Stenmark H. ER-endosome contact sites: molecular compositions and functions. *EMBO J* 2015;**34**: 1848–1858.
16. Giorgi C, De Stefani D, Bononi A, Rizzuto R, Pinton P. Structural and functional link between the mitochondrial network and the endoplasmic reticulum. *Int J Biochem Cell Biol* 2009;**41**:1817–1827.
17. Zachari M, Gudmundsson SR, Li Z, Manifava M, Cugliandolo F, Shah R, et al. Selective autophagy of mitochondria on a ubiquitin-endoplasmic-reticulum platform. *Dev Cell* 2019;**50**:627–643 e5.
18. Mito T, Vincent AE, Faitg J, Taylor RW, Khan NA, McWilliams TG, et al. Mosaic dysfunction of mitophagy in mitochondrial muscle disease. *Cell Metab* 2022;**34**:197–208 e5.
19. Gelmetti V, de Rosa P, Torosantucci L, Marini ES, Romagnoli A, di Rienzo M, et al. PINK1 and BECN1 relocalize at mitochondria--associated membranes during mitophagy and promote ER-mitochondria tethering and autophagosome formation. *Autophagy* 2017;**13**:654–669.
20. Rambold AS, Kostelecky B, Elia N, Lippincott-Schwartz J. Tubular network formation protects mitochondria from autophagosomal degradation during nutrient starvation. *Proc Natl Acad Sci U S A* 2011;**108**:10190–10195.
21. Bakay M, Wang Z, Melcon G, Schiltz L, Xuan J, Zhao P, et al. Nuclear envelope dystrophies show a transcriptional fingerprint suggesting disruption of Rb-MyoD pathways in muscle regeneration. *Brain* 2006; **129**:996–1013.
22. Zhu W, Streicher K, Shen N, Higgs BW, Morehouse C, Greenlees L, et al. Genomic signatures characterize leukocyte infiltration in myositis muscles. *BMC Med Genomics* 2012;**5**:53.
23. Perfetti A, Greco S, Fasanaro P, Bugiardini E, Cardani R, Manteiga JMG, et al. Genome wide identification of aberrant alternative splicing events in myotonic dystrophy type 2. *PLoS ONE* 2014;**9**:e93983.
24. Pescatori M, Broccolini A, Minetti C, Bertini E, Bruno C, D'amico A, et al. Gene expression profiling in the early phases of DMD: a constant molecular signature characterizes DMD muscle from early postnatal life throughout disease progression. *FASEB J* 2007;**21**:1210–1226.
25. Pelletier L, Petiot A, Brocard J, Giannesini B, Giovannini D, Sanchez C, et al. In vivo RyR1 reduction in muscle triggers a core-like myopathy. *Acta Neuropathol Commun* 2020;**8**:192.
26. Schuler M, Ali F, Metzger E, Chambon P, Metzger D. Temporally controlled targeted somatic mutagenesis in skeletal muscles of the mouse. *Genesis* 2005;**41**:165–170.
27. Millay DP, O'Rourke JR, Sutherland LB, Bezprozvannaya S, Shelton JM, Bassel-Duby R, et al. Myomaker is a membrane activator of myoblast fusion and muscle formation. *Nature* 2013;**499**:301–305.
28. Gomes LC, Scorrano L. Mitochondrial elongation during autophagy: a stereotypical response to survive in difficult times. *Autophagy* 2011;**7**:1251–1253.
29. Hemel I, Sarantidou R, Gerards M. It takes two to tango: the essential role of ER-mitochondrial contact sites in mitochondrial dynamics. *Int J Biochem Cell Biol* 2021;**141**:106101.
30. Luan P, D'Amico D, Andreux PA, Laurila PP, Wohlwend M, Li H, et al. Urolithin A improves muscle function by inducing mitophagy in muscular dystrophy. *Sci Transl Med* 2021;**13**.
31. Rizzuto R, Marchi S, Bonora M, Aguiari P, Bononi A, de Stefani D, et al. Ca^{2+} transfer from the ER to mitochondria: when, how and why. *Biochim Biophys Acta* 2009; **1787**:1342–1351.
32. Laurila PP, Luan P, Wohlwend M, Zanou N, Crisol B, Imamura de Lima T, et al. Inhibition of sphingolipid de novo synthesis counteracts muscular dystrophy. *Sci Adv* 2022;**8**:eabh4423.
33. Laurila P-P, Wohlwend M, Imamura de Lima T, Luan P, Herzig S, Zanou N, et al. Sphingolipids accumulate in aged muscle, and their reduction counteracts sarcopenia. *Nature Aging* 2022;**2**:1159–1175.
34. Hussain S, Taylor M, Waltermaurer E, McCauley J, Ford DE, Campbell JC, et al. Computer-administered screening of reproductive-aged women for diabetes risk in primary care settings, feasibility and acceptability of such screening, and validity of risk assessments based on self-reported weight. *Prev Chronic Dis* 2007;**4**:A54.
35. Nishitoh H, Ichijo H. Molecular mechanisms of ER stress-induced apoptosis. *Tanpakushitsu Kakusan Koso* 2004;**49**: 1006–1009.
36. Pennuto M, Tinelli E, Malaguti MC, del Carro U, D'Antonio M, Ron D, et al. Ablation of the UPR-mediator CHOP restores motor function and reduces demyelination in Charcot-Marie-Tooth 1B mice. *Neuron* 2008;**57**:393–405.
37. Volmer R, Ron D. Lipid-dependent regulation of the unfolded protein response. *Curr Opin Cell Biol* 2015;**33**:67–73.
38. Han J, Kaufman RJ. The role of ER stress in lipid metabolism and lipotoxicity. *J Lipid Res* 2016;**57**:1329–1338.
39. Kuma A, Matsui M, Mizushima N. LC3, an autophagosome marker, can be incorporated into protein aggregates independent of autophagy: caution in the interpretation of LC3 localization. *Autophagy* 2007;**3**: 323–328.
40. Cabrera D, Arab JP, Arrese M. UDCA, NorUDCA, and TUDCA in liver diseases: a review of their mechanisms of action and clinical applications. *Handb Exp Pharmacol* 2019;**256**:237–264.